

**Synthesis of Eu<sup>3+</sup>-doped ZnO/Bi<sub>2</sub>O<sub>3</sub> heterojunction photocatalyst on graphene oxide sheets  
for visible light-assisted degradation of 2,4-dimethyl phenol and bacteria killing**

Pooja Shandilya<sup>a,b</sup>, Anita Sudhaik<sup>a</sup>, Pankaj Raizada<sup>a,b</sup>, Ahmad Hosseini-Bandegharai<sup>c,d</sup>,  
Pardeep Singh<sup>a\*</sup>, Abolfazl Rahmani-Sani<sup>c,\*\*</sup>, Vijay Thakur<sup>e\*\*\*</sup>

<sup>a</sup>School of Chemistry, Faculty of Basic Sciences, Shoolini University, Solan(HP)-173229, India

<sup>b</sup>Himalayan Centre for Excellence in Nanotechnology, Shoolini University, Solan (HP) India-  
173229

<sup>c</sup>Department of Environmental Health Engineering, Faculty of Health, Sabzevar University of  
Medical Sciences, Sabzevar, Iran

<sup>d</sup>Department of Engineering, Kashmar Branch, Islamic Azad University, PO Box 161, Kashmar,  
Iran

<sup>e</sup>Enhanced Composites and Structures Center, School of Aerospace, Transport and  
Manufacturing, Cranfield University, Bedfordshire MK43 0AL, UK

Email: [\\*pardeepchem@gmail.com](mailto:*pardeepchem@gmail.com), [\\*\\*rahmani240@gmail.com](mailto:**rahmani240@gmail.com)),  
[\\*\\*\\*vijay.kumar@cranfield.ac.uk](mailto:***vijay.kumar@cranfield.ac.uk)

## Abstract

We reported the immobilization of binary heterojunction  $\text{Eu}^{3+}\text{-ZnO/Bi}_2\text{O}_3$  over the surface of graphene oxide (GO) sheets by precipitation method to compose a visible light drive photocatalyst.

The ternary nanocomposites were characterized by different spectral technique like FESEM, FTIR, XRD, XPS, EDX, HRTEM, UV-visible, PL, HPLC and LCMS analysis. The high specific surface area of  $106.0 \text{ m}^2\text{g}^{-1}$  of  $\text{Eu}^{3+}\text{-ZnO/Bi}_2\text{O}_3/\text{GO}$  nanocomposites was ascertained by BET adsorption-desorption isotherm. The nano-composite exhibit excellent photo-efficiency for the photodegradation of 2, 4-dimethyl phenol (DMP) under visible region and was almost completely mineralized in 100 min as compared to the bare and binary system. The mineralized products of DMP were analyzed by HPLC and LCMS analysis. The kinetic model suggests the degradation pathway obeys pseudo-first order kinetic. Their antibacterial property were assessed against *E. coli* bacteria and nearly 90% of gram negative bacteria were killed by using ternary photocatalyst as determined by CFU method. Also,  $\text{Eu}^{3+}\text{-ZnO/Bi}_2\text{O}_3/\text{GO}$  nanocomposites possessed significant recycle efficiency up to six consecutive cycles which is beneficial to minimize the tariff. The improved photo-efficiency is due to the extension towards visible region, increase surface area, and high charge separation in ternary heterojunction.

**Keywords:**  $\text{Eu}^{3+}$ -doped ZnO;  $\text{Bi}_2\text{O}_3$ ; Heterojunction formation; Enhanced photo-catalysis; 2,4-dimethylphenol degradation; Antibacterial activity

## Introduction

Phenols and their derivative is a primary pollutant released by the various industries like paint, textiles, paper, plastics, petroleum refining and pharmaceutical industries etc. [1]. The existence of phenolic compounds in waste water need to be eliminated as it brings a lots of harmful effects on human health and aquatic life. To address this, advanced oxidation processes (AOPs) have found a valuable potential for the degradation of various pollutant in aqueous suspension [2]. Amongst, AOP's process employed for the organic pollutants degradation, visible light assisted photocatalysis is of the most appropriate ones, owing to its several advantages like inexpensiveness and effectiveness. Among the various semiconductors used for photocatalytic processes, zinc oxide (ZnO) has emerged as a suitable catalyst for photocatalytic degradation and mineralization of various organic and inorganic contaminants [3]. The excellence of ZnO is due to its strong oxidizing power and low cost which makes it a favorable candidate to carry out photocatalytic oxidation processes occurring in water media [4]. On exposure to solar light with energy higher or equal to the band gap of ZnO semiconductor, generation of electron-hole pair takes place. The generated electrons reacts with  $O_2$  to form superoxide radicals ( $O_2^{\bullet-}$ ) and meanwhile, the holes reacts with  $H_2O$  or  $OH^-$  ions to produce hydroxyl radicals ( $\bullet OH$ ) [5, 6]. Owing to strong oxidizing ability,  $\bullet OH$  and  $O_2^{\bullet-}$  degraded the pollutant and convert them into  $H_2O$  and  $CO_2$  [7]. However, ZnO is only active under UV light, and it also suffers from re-combination of charge carrier produced during photocatalysis [8]. To overcome these drawbacks of ZnO and similar semiconductors, till now, two main strategy have been employed: (i) doping with cationic, anionic or rare earth elements and (ii) the construction of heterojunction with other semiconductors [9–11]. These strategy aims to enhance the stability, photocatalytic efficacy and expand the absorption of light in visible range. Nowadays, doping with a rare earth element, like  $Ln^{3+}$  ion, has

65 been revealed that can cause improvement in the ZnO photocatalytic activity [10]. Khataee *et al.*  
66 prepared Eu<sup>3+</sup> doped ZnO nanoparticles by using the sonochemical method and was exploited for  
67 the photo-degradation of acid orange dye [10]. Similarly, Aneesh et al. prepared Eu<sup>3+</sup> doped ZnO  
68 nanoparticles with various amounts of Eu-dopant, in which the luminescence quenching of ZnO  
69 nanoparticles was enhanced with increase in doping concentration of Eu [11].

70 On other hand, bismuth oxide (Bi<sub>2</sub>O<sub>3</sub>) is more advantageous and emerges as noble  
71 photocatalyst with a band gap of ~1.75–2.8 eV active under visible light region [12, 13]. It is an  
72 attractive compound with variety of application in electronics, fuel cells, ceramics, gas sensors and  
73 catalyst etc. Earlier, Bi<sub>2</sub>O<sub>3</sub> has already been utilized to boost the photocatalytic activity of metal  
74 oxide semiconductor photocatalysts. For instance, Balachandran and Swaminathan prepared a  
75 series of  $\alpha$ -Bi<sub>2</sub>O<sub>3</sub>/ZnO nanocomposites with variable amounts of  $\alpha$ -Bi<sub>2</sub>O<sub>3</sub> (6.8–18.9 wt %) and used  
76 them for photodegradation of acid red dye [14]. Similarly, Yang et al. reported the fabrication of  
77 ZnO nano-fibers and  $\beta$ -Bi<sub>2</sub>O<sub>3</sub> heterostructure and utilized it for Rhodamine B dye  
78 photodegradation under both UV and visible light [15]. Due to low band gap and high rate of  
79 recombination of bare Bi<sub>2</sub>O<sub>3</sub> photocatalyst, limits its application to use as efficient photocatalyst.  
80 Thus formation of heterojunction is an effective strategy for constructing visible light active  
81 photocatalyst and also to mitigate the rate of electron-hole pair recombination. Coupling two  
82 semiconductor with suitable energy gap and band edge potential to enhance the photoefficiency is  
83 the sole criteria for forming heterojunction Here, the valence band edge and conduction band edges  
84 of Bi<sub>2</sub>O<sub>3</sub> make it suitable for the coupling with Eu<sup>+3</sup>-ZnO.

85 Recently, carbon material is acquiring lots of attention due to their versatile properties. The  
86 various carbon derived material utilized so far as a supportive material for binary heterojunction  
87 were graphene, graphene oxide, carbon nanotube, fullerene, activated carbon etc. Large specific

surface area, high electrical and thermal conductivity, and facile charge carrier mobility make graphene oxide more advantageous to be utilized in combination with different binary and ternary heterojunction for enhanced photo-efficiency [16]. In the present work, the follow-up of our previous studies is continued in the field of graphene-based composites for photodegradation of organic contaminants in aqueous suspension.  $\text{Eu}^{3+}$  doped ZnO was coupled with  $\text{Bi}_2\text{O}_3$  which in turn dispersed onto graphene oxide (GO) surface and the fabricated composite were then utilized for photodegradation of DMP in water samples.  $\text{Eu}^{3+}$ -ZnO/ $\text{Bi}_2\text{O}_3$ /GO photocatalyst was comprehensively characterized by FESEM, TEM, XRD, EDX, UV-visible techniques, along with photoluminescence (PL) analysis. Due to the toxicity, carcinogenic nature, and resistance towards degradation of DMP, it was photodegraded by utilizing  $\text{Eu}^{3+}$ -ZnO/ $\text{Bi}_2\text{O}_3$ /GO. Further, the degradation kinetics followed by most plausible mechanism for the increased photocatalytic efficiency of the ternary heterojunction was also proposed. Lastly, recycle efficiency of  $\text{Eu}^{3+}$ -ZnO/ $\text{Bi}_2\text{O}_3$ /GO up to six catalytic cycle was also assessed for DMP degradation.

## 2. Experimental

### 2.1. Fabrication of $\text{Eu}^{3+}$ -ZnO/ $\text{Bi}_2\text{O}_3$ /GO

Here, advanced Hummer method were executed to synthesize graphene oxide as per previously reported work [16].  $\text{Eu}^{3+}$  doped ZnO was prepared using the sonochemical method [17]. Typically,  $\text{ZnCl}_2$  (1 g) and of  $\text{C}_6\text{H}_9\text{EuO}_6 \cdot x\text{H}_2\text{O}$  (0.1 g) were dissolved in 100 mL of distilled water. To this reaction mixture, NaOH (1M) was added to maintain pH 10 and the mixture was subjected to ultrasonication for 1 h. The obtained white precipitates were rinsed with ethanol and deionized water and dried at 80 °C in hot air oven. ZnO was prepared by the same procedure without addition of  $\text{C}_6\text{H}_9\text{EuO}_6 \cdot x\text{H}_2\text{O}$ . In order to prepare  $\text{Eu}^{3+}$ -ZnO/ $\text{Bi}_2\text{O}_3$ /GO, GO (1 g) was dispersed in distilled water (100 mL) with sonication for half an hour. To this suspension, 1.0 g  $\text{Bi}(\text{NO}_3)_3$  and 30 mL

NH<sub>4</sub>OH (1 M) were added with continuous stirring. In the next step, 0.5 g Eu<sup>3+</sup>-ZnO was added to the reaction solution followed by sonication for 1 h. Eventually, precipitates were separated and washed with water, dried at 80 °C to obtain Eu<sup>3+</sup>-ZnO/Bi<sub>2</sub>O<sub>3</sub>/GO composite. The same route was exploited to prepare Bi<sub>2</sub>O<sub>3</sub> with no addition of GO and Eu<sup>3+</sup>-ZnO during the course of the reaction. GO was used as support for Eu<sup>3+</sup>-ZnO/Bi<sub>2</sub>O<sub>3</sub> nanoparticles with even dispersal of Eu<sup>3+</sup>-ZnO/Bi<sub>2</sub>O<sub>3</sub> and low agglomeration over its surface.

## 2.2. Apparatus

Transmission electron microscopy (TEM) pictures was captured on a randomly selected area at voltage of 200 kV, using FP/5022-Tecnaï G2 20 S-TWIN (USA) instrument. A Nava Nano SEM-45 (USA) instrument was applied for recording the scanning electron microscopy (SEM) micrographs. A Perkin-Elmer Spectrometer (Spectrum RX-I) with KBr pellet was used for recording the FTIR spectra ranges from 4000-400 cm<sup>-1</sup>. A Panalytical's X'Pert Pro diffractometer with CuK- $\alpha$ -1 (45 kV/100 mA) source was used for recording X-ray diffraction (XRD) patterns. To estimate the optical absorption performance, using BaSO<sub>4</sub> as the reference, a diffuse reflectance spectrophotometer (UV 3600, Shimadzu) was employed. A Coulter SA3100 instrument was exploited for determination of the BET surface area of the sample by the aid of Nitrogen adsorption-desorption isotherms. A FLS-920 instrument (Edinburgh) was employed for recording the photoluminescence (PL) spectra. A digital lux-meter (750 lx) was used for the measurement of light intensity. For the analysis of degradation product during mineralization, a test were performed on a Water HPLC instrument (Austria) utilizing a C<sub>18</sub> column (5 $\mu$ m, 25cm length and 7mm diameter) and taking a 1:39:60 ratio of acetic acid: methanol: water as eluent with a flow rate of 0.5 mL min<sup>-1</sup>. The LCMS information was obtained for analyzing degradation products using JEOL GC/MATE II GC-MS with a high-resolution data system.

### 2.3. Photocatalytic activity of $\text{Eu}^{3+}\text{-ZnO/Bi}_2\text{O}_3\text{/GO}$ for DMP degradation

The photocatalytic experiment were conducted in a self-developed photoreactor. Details of photoreactor are given in our previous work [18]. The estimation of chemical oxygen demand analysis was done using the reflux technique [19].  $\text{CO}_2$  was estimated by titration of the reaction mixture with NaOH solution [20]. The DMP removal percentage was computed using Eq. (1).

$$\% \text{ removal efficiency} = \frac{C_0 - C_t}{C_0} \times 100 \quad (1)$$

Where,  $C_t$  and  $C_0$  are the instant and initial concentrations/COD of DMP, respectively.

## 3. Results and discussion

### 3.1. Morphology and structure characterization of $\text{Eu}^{3+}\text{-ZnO/Bi}_2\text{O}_3\text{/GO}$

The FESEM images of GO and  $\text{Eu}^{3+}\text{-ZnO/Bi}_2\text{O}_3\text{/GO}$  are laid out in Fig. 1 a-d. The graphene oxide exfoliation can be observed in Fig.1 a. Fig. 1b shows the thin, wrinkled, non-uniform and highly porous GO surface. The porous surface of GO facilitates the adsorption of organic pollutants present in the aqueous phase. In Fig. 1c, dispersion of  $\text{Eu}^{3+}\text{-ZnO/Bi}_2\text{O}_3$  photocatalyst onto GO surface can be clearly depicted. As can be seen in high magnification FESEM image, the agglomerates of  $\text{Eu}^{3+}\text{-ZnO/Bi}_2\text{O}_3$  are of different size and shape (Fig.1d). HRTEM analysis further ascertained the deposition of  $\text{Eu}^{3+}\text{-ZnO}$  and  $\text{Bi}_2\text{O}_3$  on porous GO sheets (Fig.2a and b). The lattice fringes at 0.33 nm, 0.28 and 0.26 nm was ascribed to (120), (001) and (002) plane of  $\text{Bi}_2\text{O}_3$ , ZnO and GO respectively [21-22]. Selected area electron diffraction (SAED) analysis confirmed the polycrystalline nature of the prepared photocatalyst (Fig. 2c). Fig. 2d explains the interplanar spacing between the two layers of  $\text{Eu}^{3+}\text{-ZnO/Bi}_2\text{O}_3\text{/GO}$  is 0.28 nm which

indicate the successful incorporation of  $\text{Eu}^{3+}\text{-ZnO/Bi}_2\text{O}_3$  over graphene oxide sheet comparable with previously reported works [22].

The XRD spectrum of  $\text{Eu}^{3+}\text{-ZnO/Bi}_2\text{O}_3/\text{GO}$  is exhibit in Fig. 3a. The diffraction peaks labeled with ♥ at  $2\theta = 26.6^\circ$ ,  $49.9^\circ$ , and  $48^\circ$  were assigned to {120}, {200} and {433} planes of  $\text{Bi}_2\text{O}_3$ , respectively [13]. The diffraction peak of GO, denoted with ♦ at  $2\theta = 26.2^\circ$ , was due to {002} plane of GO [2]. The XRD peaks leveled with ● at  $31^\circ$ ,  $34^\circ$ ,  $37^\circ$ ,  $47.6^\circ$ ,  $56^\circ$ ,  $63^\circ$ ,  $65^\circ$ , and  $70^\circ$  were assigned to {100}, {002}, {101}, {102}, {110}, {103}, {102} and {112} planes present in  $\text{Eu}^{3+}\text{-ZnO}$  [10]. FTIR spectrum of  $\text{Eu}^{3+}\text{-ZnO/Bi}_2\text{O}_3/\text{GO}$  is shown in Fig. 3b. The band at  $525\text{ cm}^{-1}$  was due to Zn-O stretching vibration [23]. The peaks at  $1405$ ,  $1650$  and  $1020\text{ cm}^{-1}$  were due to C-H (bending vibration), C=O and C-O-C stretching vibrations, respectively [24]. The peak at  $862\text{ cm}^{-1}$  was due to Bi-O stretching vibration present in  $\text{Bi}_2\text{O}_3$  [13]. The peak at  $3435$  was assigned to O-H stretching of adsorbed water molecules [25]. The atomic percentage of Zn, Bi, Eu, C and O is 6.7, 4.5, 0.54, and 55.70, 32.97 as depicted by EDX analysis (Fig. S1). The analysis of these results confirmed the formation of  $\text{Eu}^{3+}\text{-ZnO/Bi}_2\text{O}_3/\text{GO}$ .

To confirm the structural changes in GO after oxidation a Raman spectra of GO were recorded between  $500$  and  $2500\text{ cm}^{-1}$  as given in supplementary Fig. S2. The intensity of D and G band in the spectra clearly explain the formation of GO from graphite using Hummer's method. The D band determines the extent of disorder due to  $\text{sp}^3$  hybridized carbon atom and G band determines the graphitic mode due to  $\text{sp}^2$  carbon atom. The Raman spectra of graphite has two peak at  $1366\text{ cm}^{-1}$  and  $1598\text{ cm}^{-1}$  with  $I_D/I_G$  ratio 0.7. Whereas, the D and G band for GO is observed at  $1364\text{ cm}^{-1}$  and  $1607\text{ cm}^{-1}$  with  $I_D/I_G$  ratio 1.03. Broad D band is due to the addition of defects after oxidation. Further, the increase in  $I_D/I_G$  ratio from graphite to graphene oxide confirms the



incorporation of oxygen containing functional group. The observed peak is in good agreement the existing literature [26].

The XPS analysis further support the FTIR spectra. Fig. 4 displayed XPS spectra of  $\text{Eu}^{3+}$ -ZnO/ $\text{Bi}_2\text{O}_3$ /GO nanocomposites. Different elements present in nanocomposites were analyzed through XPS and provides information about chemical composition and oxidation states of different elements. Through XPS analysis, presence of Europium (Eu), Zinc (Zn), Bismuth (Bi), Oxygen (O) and Carbon (C) were confirmed in  $\text{Eu}^{3+}$ -ZnO/ $\text{Bi}_2\text{O}_3$ /GO nanocomposites. The high resolution spectra of C1s, O1s, Zn2p, Bi4f, and Eu3d core level could be observed in Fig. 4 (a-e). The binding energies at 1165 eV and 1135 eV were accredited to Eu 3d<sub>3/2</sub> and Eu 3d<sub>5/2</sub> orbital (Fig. 4a) [27]. These energy peaks confirms the presence of Eu (III) in synthesized nanocomposites. Zinc exhibited two sharp peaks at 1024 eV and 1043 eV binding energies which were assignable to Zn-2p<sub>3/2</sub> and Zn-2p<sub>1/2</sub> in Zn<sup>2+</sup> state of ZnO and shown in Fig. 4b [28]. XPS spectrum of Bi 4f (Bi 4f<sub>5/2</sub> and Bi 4f<sub>7/2</sub>) displayed in Fig. 4c possessed peaks at 158.6 and 164.5 eV [29]. Strong peak established at 530.5 eV was associated to O 1s orbital of oxygen atom (Fig. 4d) [30]. XPS spectrum of C1s showed sharp peaks at 283 and 288 eV were ascribed to sp<sup>2</sup> C-C bond and C-O bonds, respectively (Fig. 4e) [31]. The spectra confirmed the successful formation of  $\text{Eu}^{3+}$ -ZnO/ $\text{Bi}_2\text{O}_3$ /GO nanocomposites.

The UV-visible spectroscopy was utilized to assess the UV-visible light activity of  $\text{Eu}^{3+}$ -ZnO/ $\text{Bi}_2\text{O}_3$ /GO (Fig. 5a). ZnO had an absorption maximum at 368 nm with dominated absorption in the UV region [11, 15], which shows ultraviolet photo-response of ZnO. However, the absorption maximum showed a red shift and was observed at 410 nm in  $\text{Eu}^{3+}$  doped ZnO.  $\text{Bi}_2\text{O}_3$  had an absorption edge at 438 nm [11, 14, 15]. In case of  $\text{Eu}^{3+}$ -ZnO/ $\text{Bi}_2\text{O}_3$ /GO, the absorption

edge was shifted to the visible region involving a red shift in absorption maximum. Tauc's plots were plotted to find the band-gap energy of prepared photocatalyst using equation 2 [32].

$$\alpha h\nu = A(h\nu - E_g)^{n/2} \quad (2)$$

Where, index (n) can have 1, 2, 3, and 4 value for allowed direct and indirect electronic transitions, and forbidden direct and indirect ones, respectively. Also,  $h\nu$  is photon energy in Tauc equation and  $\alpha$  symbol shows absorption coefficient. The band gaps of ZnO,  $\text{Eu}^{3+}\text{-ZnO/Bi}_2\text{O}_3/\text{GO}$  and  $\text{Bi}_2\text{O}_3$  are 3.36, 3.01, and 1.8 eV, respectively (Fig. 5b). The charge separation mechanism in photocatalytic reaction was predicted by the photoluminescence analysis. ZnO had an emission peak at 375 nm (Fig. 5c). The emission peaks intensity lowered in both  $\text{Eu}^{3+}\text{-ZnO/Bi}_2\text{O}_3$  and  $\text{Eu}^{3+}\text{-ZnO/Bi}_2\text{O}_3/\text{GO}$ . The decreased intensity of PL emission peak in  $\text{Eu}^{3+}\text{-ZnO/Bi}_2\text{O}_3/\text{GO}$  displayed deferred rate of recombination as compared to  $\text{Eu}^{3+}\text{-ZnO/Bi}_2\text{O}_3$  and ZnO, respectively. This attribute to the electron engulfing nature of graphene oxide sheets towards charge carriers [2]. Fig. 5d shows nitrogen adsorption-desorption isotherms of  $\text{Eu}^{3+}\text{-ZnO/Bi}_2\text{O}_3/\text{GO}$ . The composite obeys type IV isotherm with specific area of  $106.0 \text{ m}^2/\text{g}$ . This high specific surface area is highly suitable for adsorption assisted photocatalytic degradation of the pollutant.

### 3.2. Photocatalytic activity of $\text{Eu}^{3+}\text{-ZnO/Bi}_2\text{O}_3/\text{GO}$ for DMP degradation

The photocatalytic activity of the composite was explored for the removal of DMP by the aid of LED radiation. Fig. 6a exhibits photodegradation of DMP against the irradiation time period. The simple light irradiation had no influence on the removal of DMP. The removal efficiencies of 99 %, 72 %, 51 %, 50 %, and 34 % were observed for  $\text{Eu}^{3+}\text{-ZnO/Bi}_2\text{O}_3/\text{GO}$ ,  $\text{Eu}^{3+}\text{-ZnO/Bi}_2\text{O}_3$ ,  $\text{Eu}^{3+}\text{-ZnO}$ , ZnO and GO. Thus, the efficiencies of the exanimate materials followed the order  $\text{Eu}^{3+}\text{-ZnO/Bi}_2\text{O}_3/\text{GO} > \text{Eu}^{3+}\text{-ZnO/Bi}_2\text{O}_3 > \text{Eu}^{3+}\text{-ZnO} > \text{Bi}_2\text{O}_3 > \text{GO}$ . The DMP removal experiments were also conducted under the dark condition to evaluate the percentages removed by adsorption

process. Throughout the adsorption process alone,  $\text{Eu}^{3+}\text{-ZnO/Bi}_2\text{O}_3/\text{GO}$ ,  $\text{Eu}^{3+}\text{-ZnO/Bi}_2\text{O}_3$ ,  $\text{Eu}^{3+}\text{-ZnO}$ ,  $\text{ZnO}$ , and  $\text{GO}$  had the respective efficiencies of 34, 8, 6, 9, and 32 % for DMP removal (Fig. 6b). The efficiency of the adsorbents followed the trend  $\text{Eu}^{3+}\text{-ZnO/Bi}_2\text{O}_3/\text{GO} > \text{GO} > \text{Eu}^{3+}\text{-ZnO/Bi}_2\text{O}_3 > \text{Eu}^{3+}\text{-ZnO} > \text{Bi}_2\text{O}_3$ . The obtained result showed that  $\text{Eu}^{3+}\text{-ZnO/Bi}_2\text{O}_3/\text{GO}$  had the highest photocatalysis activity as well as the adsorption capability. The GO coupling with  $\text{Eu}^{3+}\text{-ZnO/Bi}_2\text{O}_3$  increased the photo-catalytic degradation of DMP. This was because of notable adsorption of DMP onto graphene oxide sheets [16]. The kinetics of degradation were studied by Eq. (3) [33].

$$-\frac{dC}{dt} = kt \quad (3)$$

Where,  $k$  is the rate constant, and  $C$  is DMP concentration at time  $t$ . This relation can be integrated between the limits of  $(0, C_0)$  and  $(t, C)$ , from which one can have Eq. (4):

$$-\ln\left(\frac{C}{C_0}\right) = kt \quad (4)$$

The graph between  $-\ln(C/C_0)$  against time was used to find the value of rate constant.  $\text{Eu}^{3+}\text{-ZnO/Bi}_2\text{O}_3/\text{GO}$ ,  $\text{Eu}^{3+}\text{-ZnO}$ ,  $\text{Bi}_2\text{O}_3$ , and  $\text{GO}$  had the rate constant of 0.087, 0.050, 0.041, and 0.019, respectively. The  $R^2$  values obtained were in the range 0.95-0.99 which indicated that pseudo-first order kinetic model was obeyed during the degradation processes. Both photocatalytic and adsorption experiments indicated that photocatalysis of DMP was significantly affected by adsorption process. So, further experiments were undertaken to find out the effect of adsorption on DMP degradation.

### 3.3. Effect of adsorption on the photo-catalytic activity of $\text{Eu}^{3+}\text{-ZnO/Bi}_2\text{O}_3/\text{GO}$

Fig. 7 shows the effectiveness of the photocatalytic degradation of DMP, using the composites, and compare their efficacy with adsorption ability alone, which is responsible for removal process. Fig. 7 displays DMP removal under three reaction parameter. The first half of the graph display, adsorption of DMP without exposing towards light. The second half of the graph indicate simultaneous adsorption and photocatalysis (i.e. A+P process) where, 98 %, 72 %, and 32% of DMP was removed using  $\text{Eu}^{3+}\text{-ZnO/Bi}_2\text{O}_3\text{/GO}$ ,  $\text{Eu}^{3+}\text{-ZnO/Bi}_2\text{O}_3$ , and GO, respectively. However, conducting photocatalytic process after adsorption (i.e. A-P process) the removal percentage of DMP in 3 h is 50 %, 68 %, and 34 % for  $\text{Eu}^{3+}\text{-ZnO/Bi}_2\text{O}_3\text{/GO}$ ,  $\text{Eu}^{3+}\text{-ZnO/Bi}_2\text{O}_3$ , and GO, respectively. The order for various catalytic processes was revealed as:  $\text{A+P} > \text{A-P} > \text{DA}$ . During the A-P process, excessive adsorption of DMP on the surface of photocatalyst blocks penetration of light and decreases the total photoactive volume of the photocatalytic systems. The decreased photoactive volume causes a defatation of catalytic activity. By using the newly prepared composite, the concurrent adsorption and photocatalysis processes are the most efficient strategy for degrading DMP under visible light.

#### 3.4. Mineralization study and recycling performance of $\text{Eu}^{3+}\text{-ZnO/Bi}_2\text{O}_3\text{/GO}$

The complete mineralization of DMP was assessed by determining COD estimation and  $\text{CO}_2$  formation during photodegradation (Fig. 8a and b). COD was assessed using  $\text{Eu}^{3+}\text{-ZnO/Bi}_2\text{O}_3\text{/GO}$  assisted A+P process, while 65% and 64% removal were observed in the case of  $\text{Eu}^{3+}\text{-ZnO}$  and  $\text{ZnO}$ , respectively. Also, 78, 55, 20, and 2 mg/L of  $\text{CO}_2$  were estimated during mineralization of DMP using  $\text{Eu}^{3+}\text{-ZnO/Bi}_2\text{O}_3\text{/GO}$ ,  $\text{Eu}^{3+}\text{-ZnO}$ ,  $\text{Bi}_2\text{O}_3$ , and GO photocatalyst, respectively. Both COD and  $\text{CO}_2$  estimations are in agreement with each other. This confirms the complete mineralization of DMP into  $\text{CO}_2$  and  $\text{H}_2\text{O}$ .

To explore the intermediate formed during the degradation of DMP, the HPLC analysis were estimated at different time intervals of 0h, 2h, 4h, 6h, 8h, 10, respectively. After exposure to visible light, the decrease in intensity of peak at retention time nearly at 12 min was noticed for DMP as displayed in Fig 8c. Further, a group of new peaks (circled in Fig. 8c) appeared in between 2 to 4 minutes which subsequently vanished after certain time interval. The appearance of these peaks can be ascribed to the intermediates, developed during the mineralization process. In LCMS, peaks at 122, 150, 182, 108, 94, 88, 116, and 46 shown in Fig. 9d were ascribed to 2,4-DMP, 2-hydroxy-5-formylbenzaldehyde, 4-hydroxyisophthalic acid, benzoquinone, phenol, oxalic acid, Maleic acid, and formic acid, respectively.

### 3.5. Band diagram and possible degradation mechanism

In order to understand the basic mechanism of enhanced photocatalysis in  $\text{Eu}^{3+}\text{-ZnO/Bi}_2\text{O}_3/\text{GO}$ , band positions of conduction band (CB) and valance band (VB) were determined exploiting Eq. (5) and (6) [34, 35]:

$$E_{VB} = \chi - E^e + 0.5 E_g \quad (5)$$

$$E_{CB} = E_{VB} - E_g \quad (6)$$

Where,  $E_g$  represents the band gap of photocatalyst,  $E^e$  is equal to a constant value of 4.5 eV i.e. energy of free electron, and  $\chi$  is electronegativity of semiconductor. The  $E_g$  and  $\chi$  for  $\text{Eu}^{3+}\text{-ZnO}$  were 3.15 and 5.79 eV while for  $\text{Bi}_2\text{O}_3$  it was found to be 1.8 and 5.59 eV, respectively [36-38]. The locations of VB and CB in  $\text{Eu}^{3+}\text{-ZnO}$  were 2.8 and -0.35 eV, respectively [36]. The position of VB and CB in  $\text{Bi}_2\text{O}_3$  was found to be 1.30 and -0.54 eV, respectively [38]. The band position of  $\text{Eu}^{3+}\text{-ZnO}$  and  $\text{Bi}_2\text{O}_3$  was suited for formation of type II heterojunction with staggered band position. The scavenging examinations were conducted by utilizing isopropyl alcohol (IPA),

benzoquinone (BZQ), ammonium oxalate (AO), and Cr(VI) ion as hydroxyl radicals ( $\text{OH}^\bullet$ ), superoxide radicals ( $\text{O}_2^{\bullet-}$ ), holes ( $\text{h}^+_{\text{VB}}$ ) and electrons ( $\text{e}^-_{\text{CB}}$ ) scavengers, respectively [39]. The removal efficiencies of 20, 54, 92, and 95 % were recorded in IPA, BZQ, Cr(VI), and AO, respectively as shown in (Fig. S3). The presence of Cr(VI) and AO had no remarkable influence on photocatalytic activity of  $\text{Eu}^{3+}\text{-ZnO/Bi}_2\text{O}_3/\text{GO}$ . During the scavenging experiment, whereas,  $\text{OH}^\bullet$  and  $\text{O}_2^{\bullet-}$  radicals showed the highest oxidizing strength for the degradation of DMP. The mechanism through which the new photocatalyst can mineralize DMP can be explained as follows (Fig. 9). Under visible light, holes, and electrons were produced in valance and conduction band of ZnO and  $\text{Bi}_2\text{O}_3$  semiconductor, respectively. The migration of charge carrier takes place from the VB of  $\text{Eu}^{3+}\text{-ZnO}$  to VB of  $\text{Bi}_2\text{O}_3$  in accordance with the position of its band potential. The band position of  $\text{Eu}^{3+}\text{-ZnO}$  and  $\text{Bi}_2\text{O}_3$  was suited for formation of type II heterojunction with staggered band position. At the same time, photo-excited electrons migrate from CB of  $\text{Bi}_2\text{O}_3$  to CB of  $\text{Eu}^{3+}\text{-ZnO}$  [40]. Due to this transfer, the recombining rate of photo-generated electron-hole pairs was diminished to a greater extent. The reaction of CB electrons of ZnO with adsorbed molecular  $\text{O}_2$  led to production of superoxide ( $\text{O}_2^{\bullet-}$ ) radicals on the surface. The hole in VB of  $\text{Bi}_2\text{O}_3$  reacts with the  $\text{H}_2\text{O}$  molecule to produce hydroxyl radicals. The hydroxyl radicals and superoxide ultimately oxidized DMP into  $\text{CO}_2$  and  $\text{H}_2\text{O}$ . Based on the obtained results,  $\text{Eu}^{3+}\text{-ZnO/Bi}_2\text{O}_3/\text{GO}$  emerged as a potential photo-catalyst for degradation of DMP present in water.

Recycling efficiency of the photocatalyst is very crucial for its long-term application in water purification process. The photo-catalyst was separated after each cycle thorough centrifugation process and utilized for the next photocatalytic cycle. After six catalytic cycles, the photo-efficiency of  $\text{Eu}^{3+}\text{-ZnO/Bi}_2\text{O}_3/\text{GO}$  was reduced from 98 to 89% (Fig. S4a). Furthermore, XRD, EDX and FITR analysis of  $\text{Eu}^{3+}\text{-ZnO/Bi}_2\text{O}_3/\text{GO}$  was performed (Fig. S4(b-d)). XRD, EDX

and FTIR spectra of  $\text{Eu}^{3+}\text{-ZnO/Bi}_2\text{O}_3\text{/GO}$  did not show any significant change in the crystalline structure of the ternary heterojunction even after six catalytic cycles. It indicates the long-term stability of prepared photocatalyst for DMP degradation.

### 3.6. Photocatalytic antibacterial activity of $\text{Eu}^{3+}\text{-ZnO/Bi}_2\text{O}_3\text{/GO}$

The photocatalytic antibacterial activity of  $\text{Eu}^{3+}\text{-ZnO/Bi}_2\text{O}_3\text{/GO}$  was assessed using *E. coli* as model bacterium under visible light. As shown in Fig 10a the percentage killing dramatically increased to 90%, on exposure of photocatalyst towards the source of visible light for 60 min. However, 10 % cell viability of *E. coli* were observed for 3 mg/ml of  $\text{Eu}^{3+}\text{-ZnO/Bi}_2\text{O}_3\text{/GO}$  under visible light Fig. 10b. The results clearly indicates the strong antibacterial activity of ternary photocatalyst against gram negative strains. Generation of ROS ( $e^-$ ,  $h^+$ ,  $\text{O}_2^{\bullet-}$ ,  $\text{OH}^\bullet$ ) during the photocatalytic process plays a crucial role in photocatalytic antibacterial performance [41]. Thus, to explore the role of generated ROS, scavenging experiments were performed to traps the ROS as shown in Fig. 10c. Isopropyl alcohol, ammonium oxalate, Cr(VI), and benzoquinone were used as scavengers for hydroxyl radical, holes, electron, and superoxide radical anion, respectively [42-43]. It can be clearly depicted from Fig. 10c that hydroxyl radical and superoxide radical were the chief oxidizing species responsible for antibacterial activity on 0.5mM optimized scavenging concentration [16]. Addition of isopropanol and benzoquinone traps the  $\text{OH}^\bullet$  and  $\text{O}_2^{\bullet-}$  from the reaction system, thus found very small decrease in cell viability.

## 4. Conclusion

In summary,  $\text{Eu}^{3+}\text{-ZnO/Bi}_2\text{O}_3\text{/GO}$  a ternary heterojunction was successfully fabricated via precipitation method. The photocatalytic efficiency of type-II heterojunction were evaluated against DMP and antibacterial property were assessed against *E. coli* under visible light source. Doping of ZnO with  $\text{Eu}^{3+}$  lowers the band gap of ZnO as compared to un-doped ZnO, further confirmed by band gap analysis. In the ternary heterojunction  $\text{Bi}_2\text{O}_3$  and graphene oxide sheets traps electron from ZnO conduction band, thereby decreasing rate of recombination as validate by PL results. Moreover, integration of  $\text{Eu}^{3+}\text{-ZnO}$  with  $\text{Bi}_2\text{O}_3$  extend the absorption towards visible region. With

the simultaneous adsorption and photodegradation (A+P) process, the novel ternary heterojunction was capable of degrading 98 % of DMP in 100 min. Nearly, 78% of CO<sub>2</sub> removal were estimated for DMP mineralization which further aid the mineralization process. The extent of mineralization also established by HPLC and LCMS analysis. Similarly, nearly 90% of *E. coli* were killed when the photocatalyst were exposed to visible light source for 60 min. The mineralization obeys pseudo-first order model. Further, scavenging experiments reveals that OH<sup>•</sup> and O<sub>2</sub><sup>•-</sup> were the principal oxidizing species responsible for mineralization. Also, the nanocomposites were recyclable up to six consecutive cycles this maintain the cost effectiveness of the photocatalyst. Thus, Eu<sup>3+</sup>-ZnO/Bi<sub>2</sub>O<sub>3</sub>/GO nanocomposites can be easily applied for the detoxification of pollutant present in water.

#### References:

- [1] P. Shandilya, D. Mittal, M. Soni, P. Raizada, A. Hosseini-Bandegharai, A.K. Saini, P. Singh, Fabrication of fluorine doped graphene and SmVO<sub>4</sub> based dispersed and adsorptive photocatalyst for abatement of phenolic compounds from water and bacterial disinfection, J. Clean. Prod. 203 (2018) 386-399.
- [2] P. Shandilya, D. Mittal, A. Sudhaik, M. Soni, P. Raizada, A.K. Saini, P. Singh, GdVO<sub>4</sub> modified fluorine doped graphene nanosheets as dispersed photocatalyst for mitigation of phenolic compounds in aqueous environment and bacterial disinfection, Sep. Purif. Technol. 210 (2019) 804-816.
- [3] B. Pare, S.B. Jonnalagadda, H. Tomar, P. Singh, V.W. Bhagwat, ZnO assisted photocatalytic degradation of acridine orange in aqueous solution using visible irradiation, Desalin. 232 (2008) 80-90.



- [4] P. Carroll, A. Myles, B. Quilty, D.E. McCormack, R. Fagan, S.J. Hinder, D.D. Dionysiou, S.C. Pillai, Antibacterial properties of F-doped ZnO visible light photocatalyst, *J. Hazard. Mater.* 324 (2017) 39-47.
- [5] S. Gautam, P. Shandilya, V.P. Singh, P. Raizada, P. Singh, Solar photocatalytic mineralization of antibiotics using magnetically separable  $\text{NiFe}_2\text{O}_4$  supported onto graphene sand composite and bentonite, *J. Water Process Eng.* 14 (2016) 86-100.
- [6] Y. Yuan, G.F. Huang, W.Y. Hu, D.N. Xiong, B.X. Zhou, S. Chang, W.Q. Huang, Construction of  $\text{g-C}_3\text{N}_4/\text{CeO}_2/\text{ZnO}$  ternary photocatalysts with enhanced photocatalytic performance, *J Phys. Chem. of Solids.* 106 (2017) 1-9.
- [7] J.H. Xiao, W.Q. Huang, Y.S. Hu, F. Zeng, Q.Y. Huang, B.X. Zhou, A. Pan, K. Li, G.F. Huang, Facile in situ synthesis of wurtzite  $\text{ZnS}/\text{ZnO}$  core/shell heterostructure with highly efficient visible-light photocatalytic activity and photostability, *J Phys. D Appl. Phys.* 51(7) (2018) 075501.
- [8] P. Raizada, P. Singh, A. Kumar, G. Sharma, B. Pare, S.B. Jonnalagadda, P. Thakur, Solar photocatalytic activity of nano-ZnO supported on activated carbon or brick grain particles: role of adsorption in dye degradation, *Appl. Catal. A*, 486 (2014) 159-169.
- [9] O. Yayapao, T. Thongtem, A. Phuruangrat, S. Thongtem, Sonochemical synthesis of Dy-doped ZnO nanostructures and their photocatalytic properties, *J. Alloys Comp.* 576 (2013) 72-79.
- [10] A.R. Khataee, A. Karimi, R.D.C. Soltani, M. Safarpour, Y. Hanifehpour, S.W. Joo, Europium-doped ZnO as a visible light responsive nanocatalyst: Sonochemical synthesis, characterization and response surface modeling of photocatalytic process, *Appl. Catal. A: Gen.* 488 (2014) 160–170.

- [11] P. M. Aneesh, M. K. Jayaraj, Red luminescence from hydrothermally synthesized Eu-doped ZnO nanoparticles under visible excitation, *Bull. Mater. Sci.* 33 (2010) 227–231.
- [12] A. Hernandez-Gordillo, J.C. Medina, M. Bizarro, R. Zanella, B.M. Monroy, S.E. Rodil, Photocatalytic activity of enlarged microrods of alpha-Bi<sub>2</sub>O<sub>3</sub> produced using ethylenediamine-solvent, *Ceram Int.* 42(10) (2016) 11866–75.
- [13] B. Priya, P. Raizada, N. Singh, P. Thakur, P. Singh, Adsorptional photocatalytic mineralization of oxytetracycline and ampicillin antibiotics using Bi<sub>2</sub>O<sub>3</sub>/BiOCl supported on graphene sand composite and chitosan, *J. Colloid Interface Sci.* 479 (2016) 271-283.
- [14] S. Balachandran, M. Swaminathan, Facile fabrication of heterostructured Bi<sub>2</sub>O<sub>3</sub>–ZnO photocatalyst and its enhanced photocatalytic activity, *J. Phys. Chem. C*, 116 (50) (2012) 26306-12.
- [15] Y. Yang, L. Xu, C. Su, J. Che, W. Sun, H. Gao, Electrospun ZnO/Bi<sub>2</sub>O<sub>3</sub> nanofibers with enhanced photocatalytic activity, *J Nanomater.* 2014 (2014) 7.
- [16] P. Shandilya, D. Mittal, M. Soni, P. Raizada, J.H. Lim, D.Y. Jeong, D.P. Dewedi, A.K. Saini, P. Singh, Islanding of EuVO<sub>4</sub> on high-dispersed fluorine doped few layered graphene sheets for efficient photocatalytic mineralization of phenolic compounds and bacterial disinfection, *J. Taiwan Inst. Chem. Eng.* (2018) 1-15.
- [17] A. Khataee, A. Karimi, M. Zarei, S.W. Joo, Eu-doped ZnO nanoparticles: Sonochemical synthesis, characterization, and sonocatalytic application *Ultrason. Sonochem.* 2015.
- [18] P. Raizada, J. Kumari, R. Dhiman, V. P. Singh, P. Singh, Magnetically retrievable Bi<sub>2</sub>WO<sub>6</sub>/Fe<sub>3</sub>O<sub>4</sub> immobilized on graphene sand composite for investigation of photocatalytic mineralization of oxytetracycline and ampicillin, *Proc. Safety Environ. Prot.* 106 (2016) 104-116.

- [19] APHA, Standard methods for examination of water and wastewater, American Public Health Association, American Water Works Association, Water Environment Federation New York, 6th Edn (1985) 535.
- [20] M. Kolb, M. Bahadir, B. Teichgräber, Determination of chemical oxygen demand (COD) using an alternative wet chemical method free of mercury and dichromate, *Water Res.* 122 (2017) 645-654.
- [21] S. Yi, X. Yue, D. Xu, Z. Liu, F. Zhao, D. Wang, Y. Lin, Study on photogenerated charge transfer properties and enhanced visible-light photocatalytic activity of p-type  $\text{Bi}_2\text{O}_3$ /n-type ZnO heterojunctions, *New J. Chem.* 39 (2015) 2917-2924.
- [22] B. Priya, P. Shandilya, P. Raizada, P. Thakur, N. Singh, P. Singh, Photocatalytic mineralization and degradation kinetics of ampicillin and oxytetracycline antibiotics using graphene sand composite and chitosan supported  $\text{BiOCl}$ , *J. Mol. Catal. A: Chem.* 423 (2016) 400-413.
- [23] R. Zhou, Q. Zhao, K.K. Liu, Y.J. Lu, L. Dong, C.X. Shan, Europium-decorated ZnO quantum dots as a fluorescent sensor for the detection of ananthrax biomarker, *J. Mater. Chem. C*, 5 (2017) 1685.
- [24] T.V.L Thejaswini, D. Prabhakaran, M.A. Maheswari, Ultrasound assisted synthesis of nano-rod embedded petal designed  $\alpha\text{-Bi}_2\text{O}_3\text{-ZnO}$  nanoparticles and their ultra-responsive visible light induced photocatalytic properties, *J. Photochem. Photobiol. A: Chem.* 335 (2017) 217-229.
- [25] P. Singh, S. Gautam, P. Shandilya, B. Priya, V.P. Singh, P. Raizada, Graphene bentonite supported  $\text{ZnFe}_2\text{O}_4$  as super-paramagnetic photocatalyst for antibiotic degradation. *Adv. Mater. Lett.* 8(3) (2017) 229-238.

- [26] S. Perumbilavil, P. Sankar, T.R. Priya, R. Philip, White light Z-scan measurements of ultrafast optical nonlinearity in reduced graphene oxide nanosheets in the 400–700 nm region. *Appl. Phys. Lett.* 107(5) (2015) 051104.
- [27] S. Kumar, R. Prakash, and Vivek K. Singh, Synthesis, characterization, and applications of europium oxide: a review, *Rev. Adv. Sci. Eng.* 4 (2015) 247-257.
- [28] S. Kumar, A. Dhiman, P. Sudhagar, V. Krishnan, ZnO-graphene quantum dots heterojunctions for natural sunlight-driven photocatalytic environmental remediation, *Appl. Surf. Sci.* 447 (2018) 802-815.
- [29] Y. Feng, L. Li, J. Li, J. Wang, L. Liu, Synthesis of mesoporous BiOBr 3D microspheres and their photodecomposition for toluene, *J. Hazard. Mater.* 192, (2011) 538-544.
- [30] H. Y. Ji, X. C. Jing, Y. G. Xu, J. Yan, H. P. Li, Y. P. Li, Y. Huang, Q Zhang, H. Xu and H. M. Li, Magnetic g-C<sub>3</sub>N<sub>4</sub>/NiFe<sub>2</sub>O<sub>4</sub> hybrids with enhanced photocatalytic activity, *RSC Adv.* 5 (2015) 57960-57967.
- [31] X.J. Wang, W.Y. Yan, F.T. Li, Y.B. Xue, R.H. Liu and Y.J. Hao, In situ microwave-assisted synthesis of porous N-TiO<sub>2</sub>/g-C<sub>3</sub>N<sub>4</sub> heterojunctions with enhanced visible-light photocatalytic properties, *Ind. Eng. Chem. Res.*, 52 (2013) 17140–17150.
- [32] P. Raizada, J. Kumari, P. Shandilya, P. Singh, Kinetics of photocatalytic mineralization of oxytetracycline and ampicillin using activated carbon supported ZnO/ZnWO<sub>4</sub> nanocomposite in simulated waste water, *Desalin. Water Treat.* 79 (79) (2017) 204-213.
- [33] P. Raizada, B. Priya, P. Thakur, P. Singh, Solar light induced photodegradation of oxytetracycline using Zr doped TiO<sub>2</sub>/CaO based nanocomposite, *Ind. J. Chem. Sec. A*, 55(7) (2016) 803-809.

- [34] J. He, Y. Cheng, T. Wang, D. Feng, L. Zheng, D. Shao, W. Wang, W. Wang, F. Lu, H. Dong, R. Zheng, H. Liu, Enhanced photocatalytic performances and magnetic recovery capacity of visible-light-driven Z-scheme  $\text{ZnFe}_2\text{O}_4/\text{AgBr}/\text{Ag}$  photocatalyst, *Appl. Surf. Sci.* 440 (2018) 99-106.
- [35] G. Gupta, A. Kaur, A.S.K. Sinha, S.K. Kansal, Photocatalytic degradation of levofloxacin in aqueous phase using  $\text{Ag}/\text{AgBr}/\text{BiOBr}$  microplates under visible light, *Mater. Res. Bull.* 88 (2017) 148–155.
- [36] C.B. Ong, L.Y. Ng, A.W. Mohammad, A review of ZnO nanoparticles as solar photocatalysts: Synthesis, mechanisms and applications, *Renewable and Sustainable Energy Reviews* 81 (2018) 536-551.
- [37] M. Han, T. Sun, P.Y. Tan, X. Chen, O.K. Tan, M.S. Tse,  $\text{m-BiVO}_4@ \gamma\text{-Bi}_2\text{O}_3$  core-shell p-n heterogeneous nanostructure for enhanced visible-light photocatalytic performance, *RSC Adv.* 3 (2013) 24964-24970.
- [38] J.C. Medina, N.S. Portillo-Velez, M. Bizarro, A. Hernández-Gordillo, S.E. Rodil, Synergistic effect of supported  $\text{ZnO}/\text{Bi}_2\text{O}_3$  heterojunctions for photocatalysis under visible light, *Dyes and Pigments* 153 (2018) 106–116.
- [39] A. Mehdinia, M. Ahmadifar, M.O. Aziz-Zanjani, A. Jabbari, M.S. Hashtroudi, Selective adsorption of 2, 4-dinitrophenol on molecularly imprinted nanocomposites of mesoporous silica SBA-15/polyaniline. *Analyst*, 137(18) (2012) 4368-4374.
- [40] L.S. Andrade, E.A. Laurindo, R.V.D. Oliveira, R.C. Rocha-Filho, Q.B. Cass, Development of a HPLC method to follow the degradation of phenol by electrochemical or photo-electrochemical treatment. *J. Braz. Chem. Soc.*, 17(2) (2006) 369-373.

- [41] P. Raizada, A. Sudhaik, P. Shandilya, A. Saini, V. Gupta, P. Singh, Fabrication of  $\text{Ag}_3\text{VO}_4$  decorated phosphorus and sulphur co-doped graphitic carbon nitride as high-dispersed photocatalyst for phenol mineralization and *E.Coli* disinfection, Sep. Purify.Technol. 212 (2018) 887-900.
- [42] P. Raizada, A. Sudhaik, P. Singh, P. Shandilya, P. Thakur, H. Jung. Visible light assisted photodegradation of 2, 4-dinitrophenol using  $\text{Ag}_2\text{CO}_3$  loaded phosphorus and sulphur co-doped graphitic carbon nitride nanosheets in simulated wastewater. Arab. J. Chem. (2018).
- [43] P. Singh, P. Raizada, A. Suadhik, P. Shandilya, P. Thakur, S. Agarwal, V.K. Gupta, Enhanced photocatalytic activity and stability of  $\text{AgBr/BiOBr/graphene}$  heterojunction for phenol degradation under visible light, J Saudi Chem. Soc. 23 (2018) 586-599.

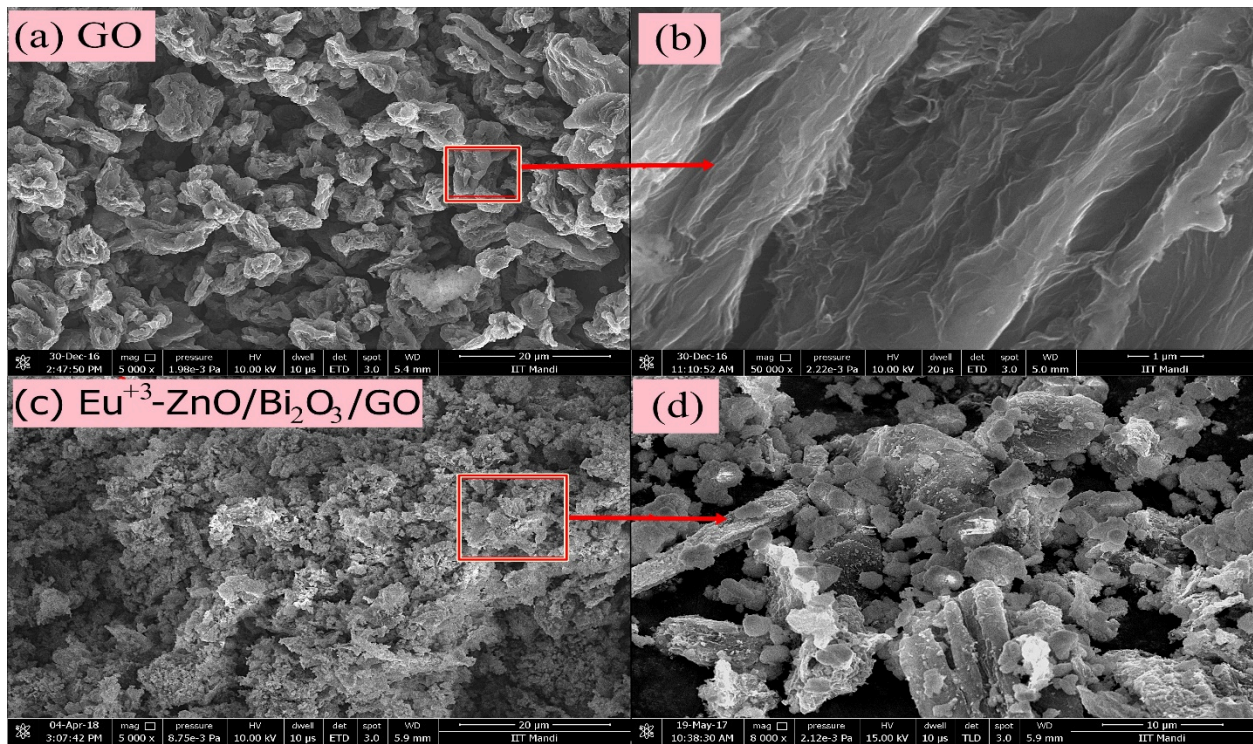


**Fig. 1.** FESEM images of (a) GO (b) magnified image of selected portion of (a), (c) Eu<sup>3+</sup>-ZnO/Bi<sub>2</sub>O<sub>3</sub>/GO and (d) magnified image of selected portion of (c).

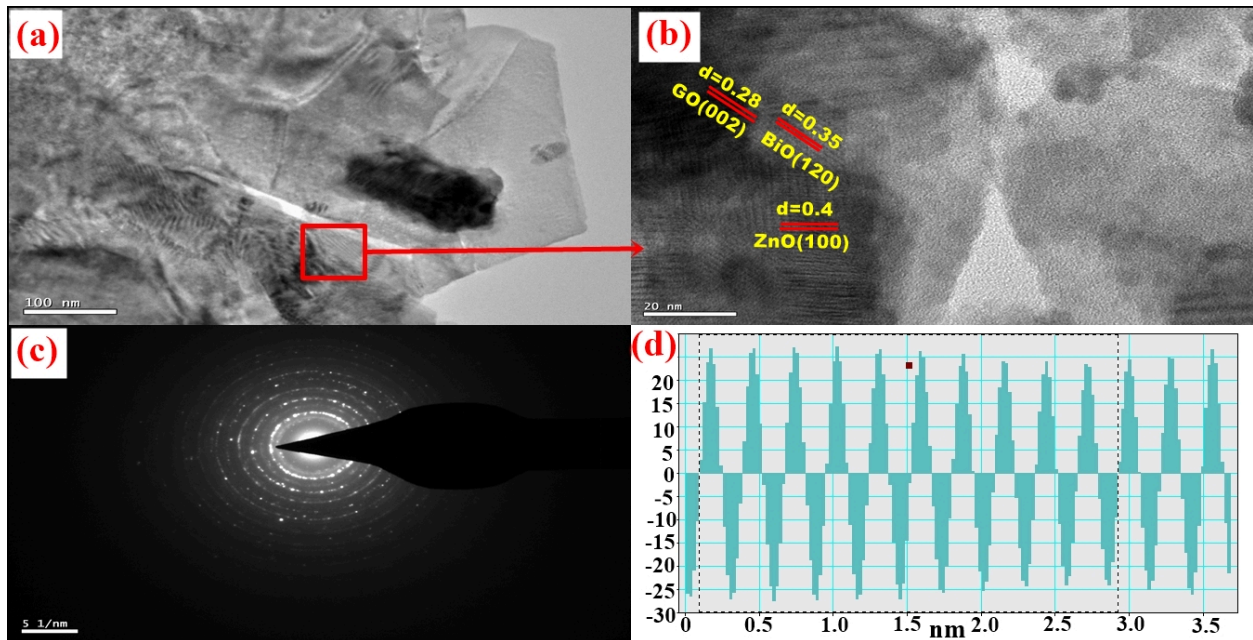


**Fig. 2.** (a) TEM images of Eu<sup>3+</sup>-ZnO/Bi<sub>2</sub>O<sub>3</sub>/GO (b) magnified image of selected portion of (a), (c) SAED pattern of Eu<sup>3+</sup>-ZnO/Bi<sub>2</sub>O<sub>3</sub>/GO and (d) planar spacing of the composite.

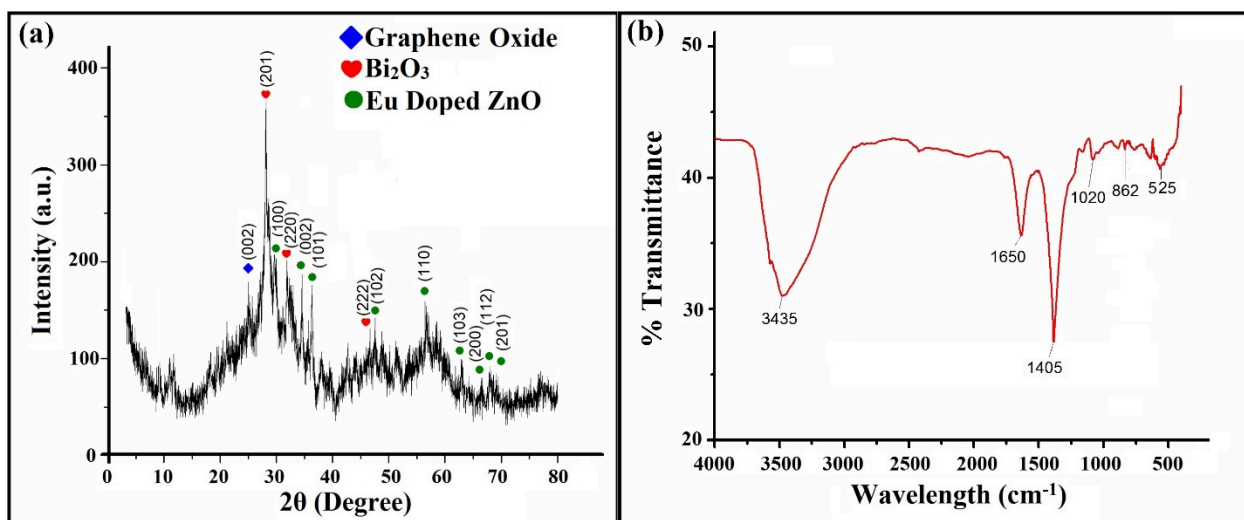


Fig. 3. XRD and FTIR spectra of  $\text{Eu}^{3+}\text{-ZnO/Bi}_2\text{O}_3/\text{GO}$  nanocomposite.

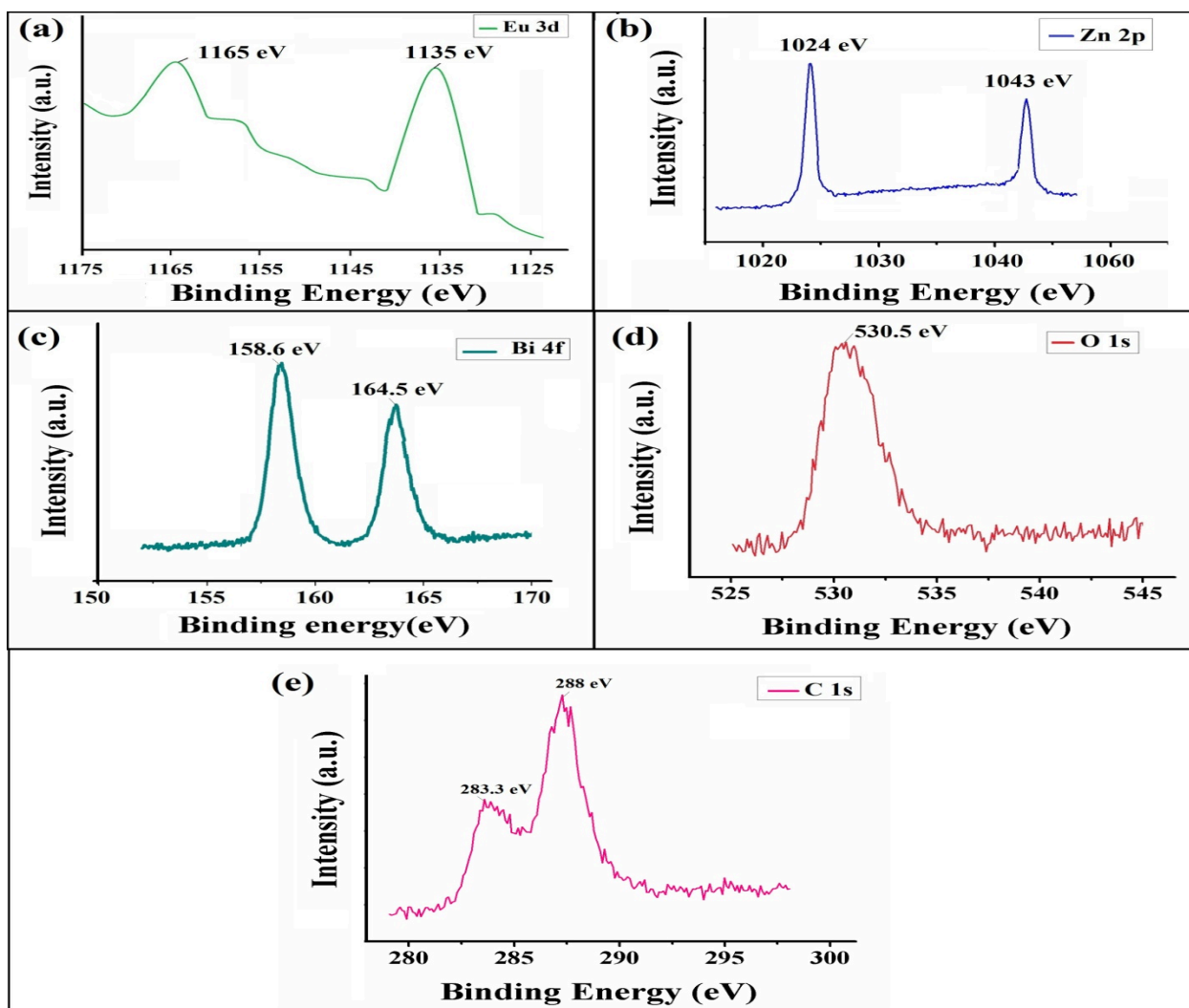
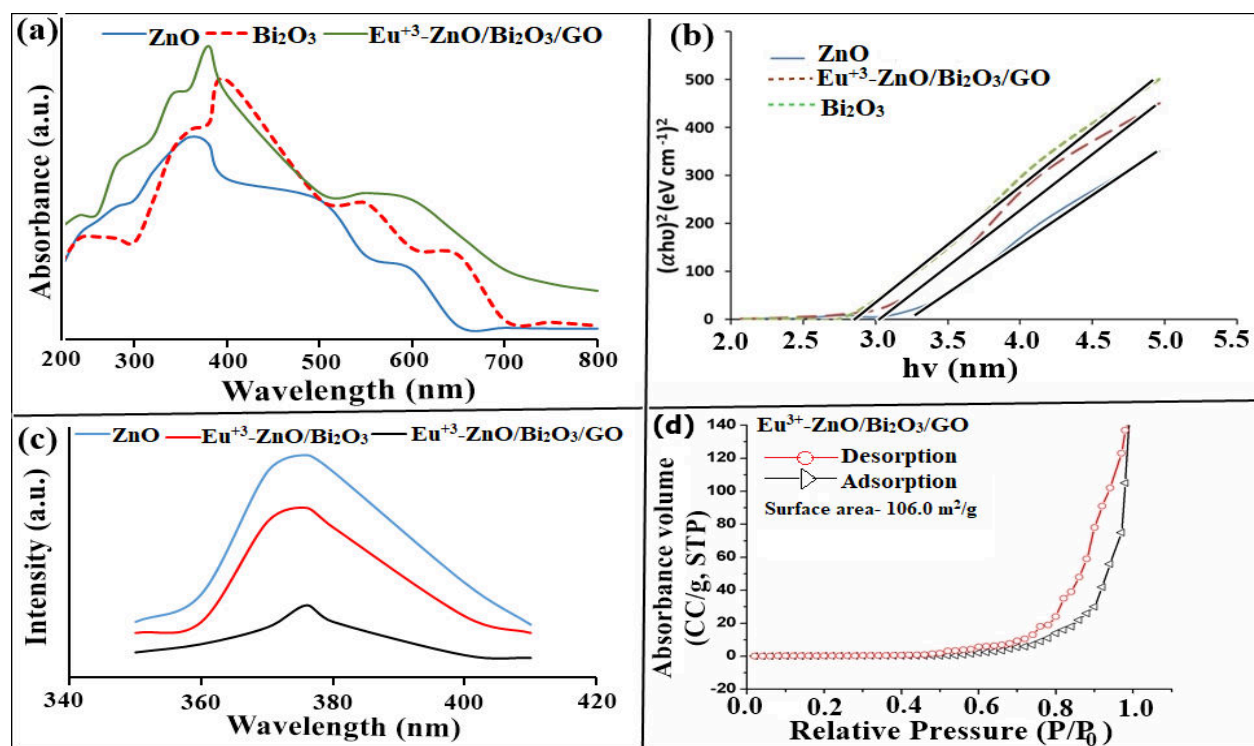
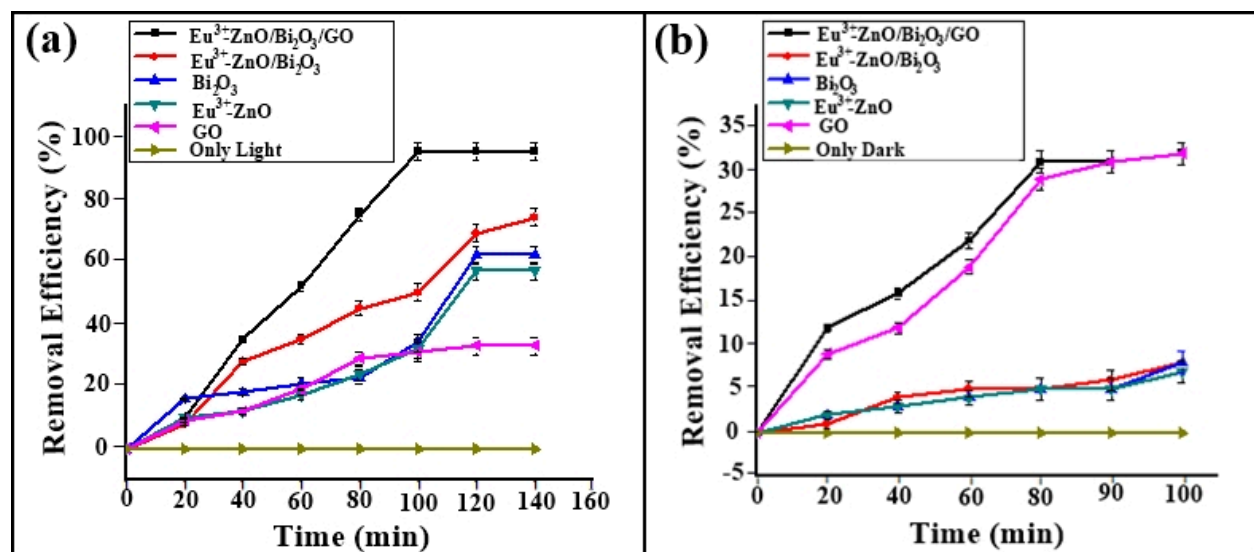


Fig. 4. XPS spectra of  $\text{Eu}^{3+}\text{-ZnO/Bi}_2\text{O}_3/\text{GO}$  nanocomposite.





**Fig. 5.** (a) UV-visible analysis, (b) Band gap calculation, (c) photoluminescence analysis and (d) BET adsorption-desorption isotherms of  $\text{Eu}^{3+}\text{-ZnO/Bi}_2\text{O}_3/\text{GO}$ .



**Fig. 6.** (a) Photocatalytic degradation of DMP and (b) adsorptional removal of DMP using  $\text{Eu}^{3+}\text{-ZnO/Bi}_2\text{O}_3/\text{GO}$  [Reaction conditions: initial reaction pH= 4.0;  $[\text{DMP}] = 1 \times 10^{-3} \text{ mol dm}^{-3}$ ; [photocatalyst] = 50 mg/100 mL; and intensity of light = 750 lx].

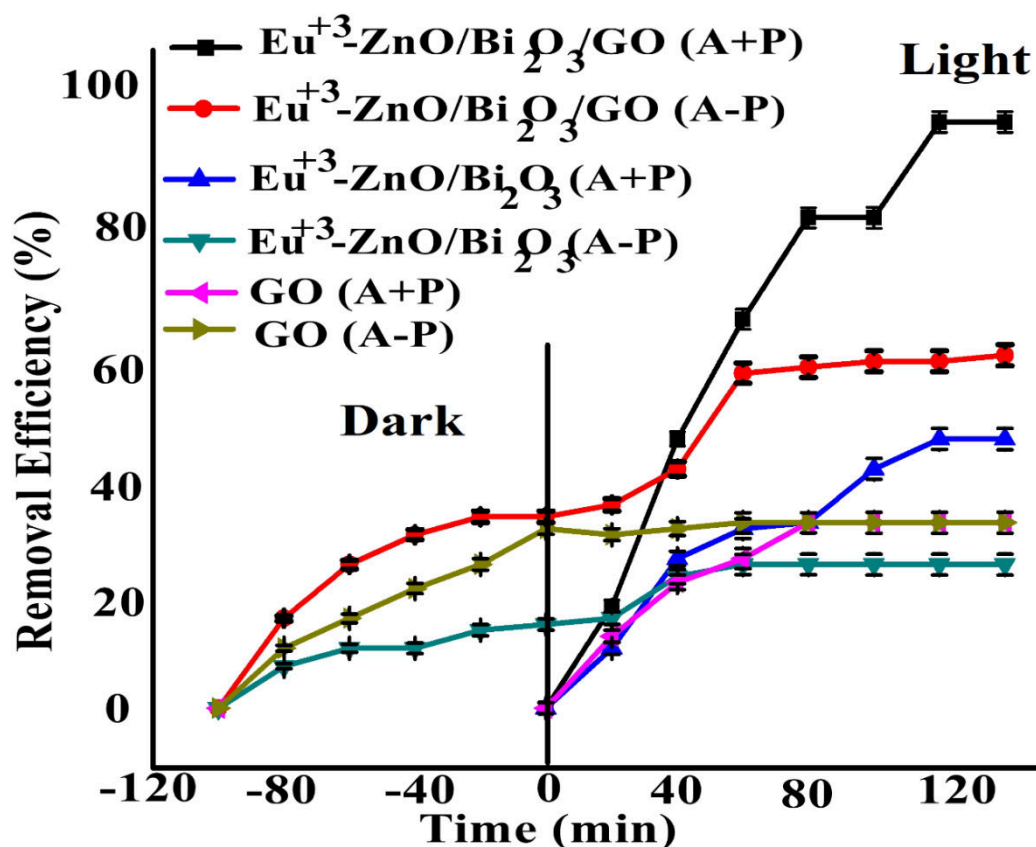


**Fig. 7.** Effect of adsorption on photodegradation of DMP using  $\text{Eu}^{3+}\text{-ZnO/Bi}_2\text{O}_3/\text{GO}$ . [Reaction conditions: initial reaction pH= 4.0;  $[\text{DMP}] = 1 \times 10^{-3} \text{ mol dm}^{-3}$ ; [photocatalyst] = 50 mg/100 mL; and intensity of light = 750 lx].

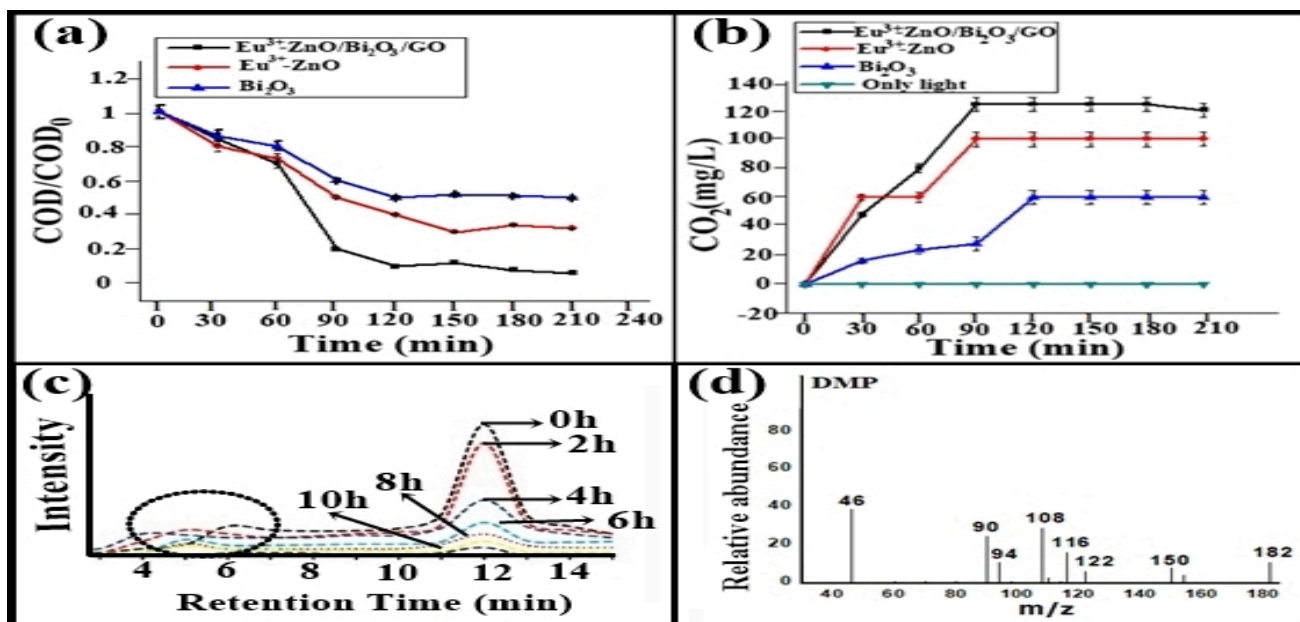


**Fig. 8.** (a) COD removal (b) CO<sub>2</sub> estimation, (c) HPLC and (d) LCMS analysis of Eu<sup>3+</sup> ZnO/Bi<sub>2</sub>O<sub>3</sub>/GO [Reaction conditions: initial reaction pH= 4.0; [DMP] = 1 × 10<sup>-3</sup> mol dm<sup>-3</sup>; [photocatalyst] = 50 mg/100 mL; and intensity of light = 750 lx].

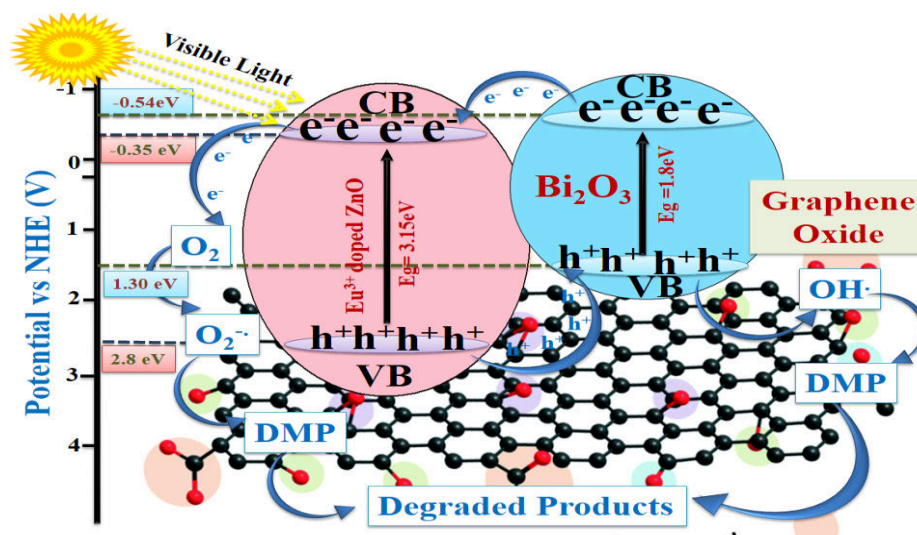


**Fig. 9.** Mechanistic view for enhanced photocatalytic degradation of DMP

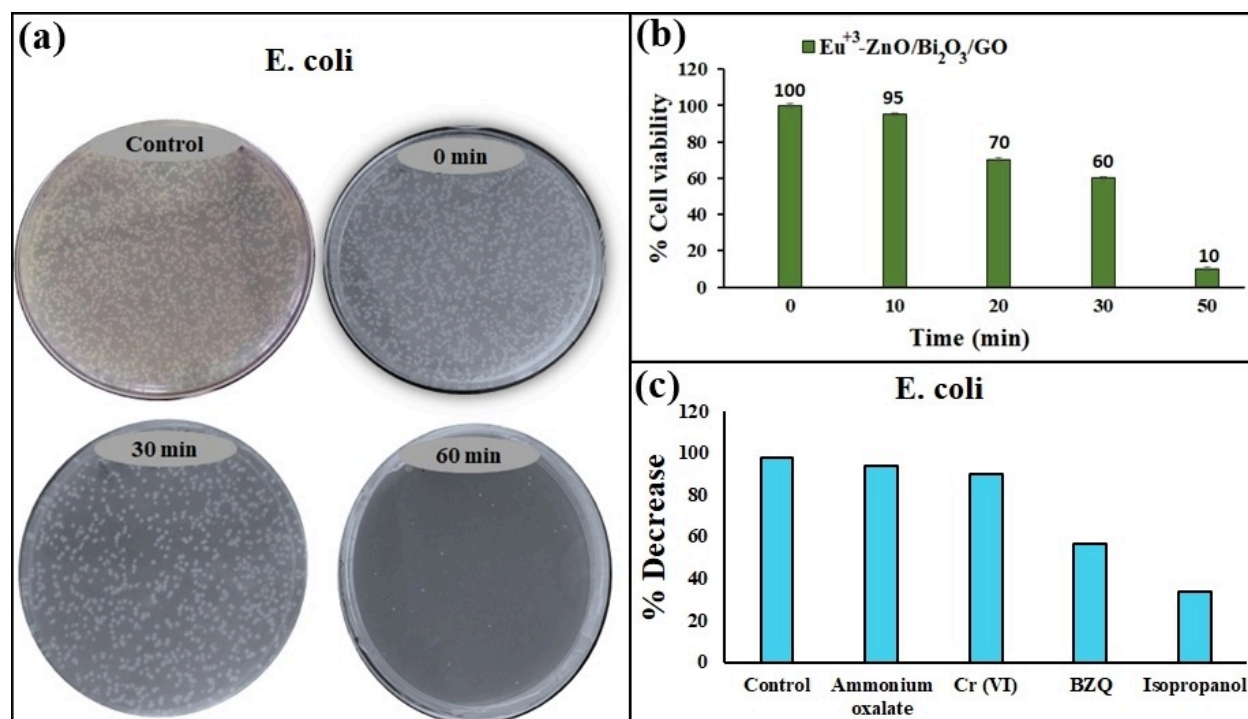


**Fig. 10.** (a) Antibacterial study of Eu<sup>3+</sup>-ZnO/Bi<sub>2</sub>O<sub>3</sub>/GO against *E. coli* by CFU method in the presence of visible light, (b) percentage cell viability under different time of light exposure of

Eu<sup>+3</sup>-ZnO/Bi<sub>2</sub>O<sub>3</sub>/GO, (c) Effect of radical scavengers on photocatalytic antibacterial activity of Eu<sup>+3</sup>-ZnO/Bi<sub>2</sub>O<sub>3</sub>/GO. [Reaction time = 1 h; light intensity = 750 lx; (c) Scavenger concentration: 0.5mM of isopropanol, benzoquinone, ammonium oxalate, Cr(VI) for 0.5 mg/ml of Eu<sup>+3</sup>-ZnO/Bi<sub>2</sub>O<sub>3</sub>/GO under solar light irradiation].

Supplementary Figures (SSSCIE\_2020\_148R2)

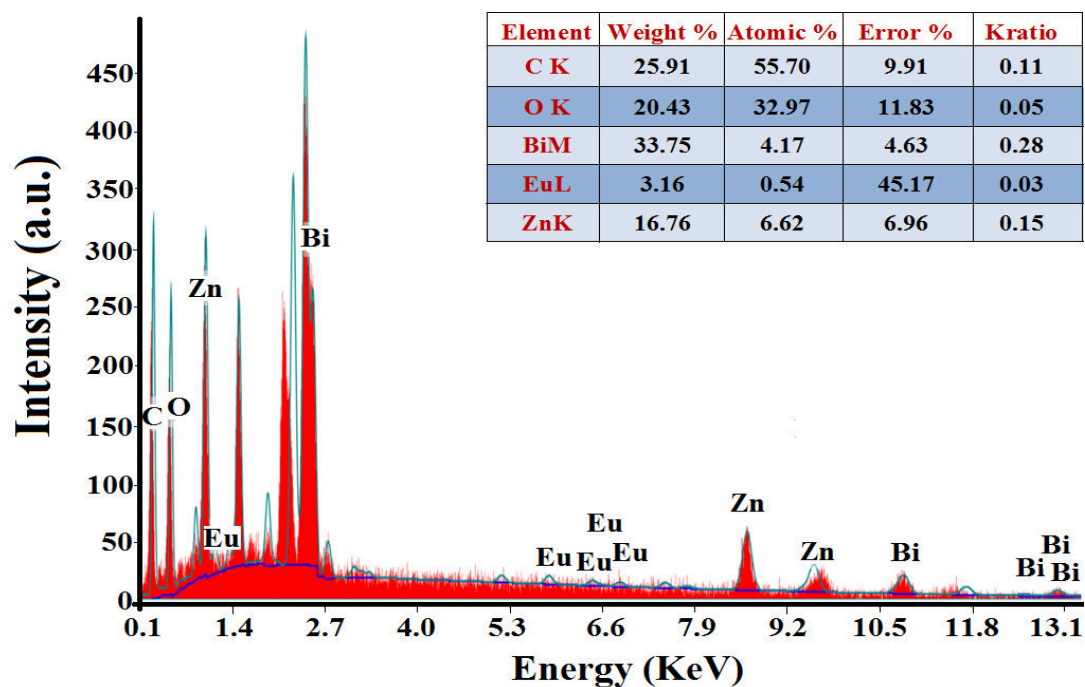


Fig. S1. EDX spectrum of  $\text{Eu}^{3+}\text{-ZnO/Bi}_2\text{O}_3/\text{GO}$  nanocomposite.

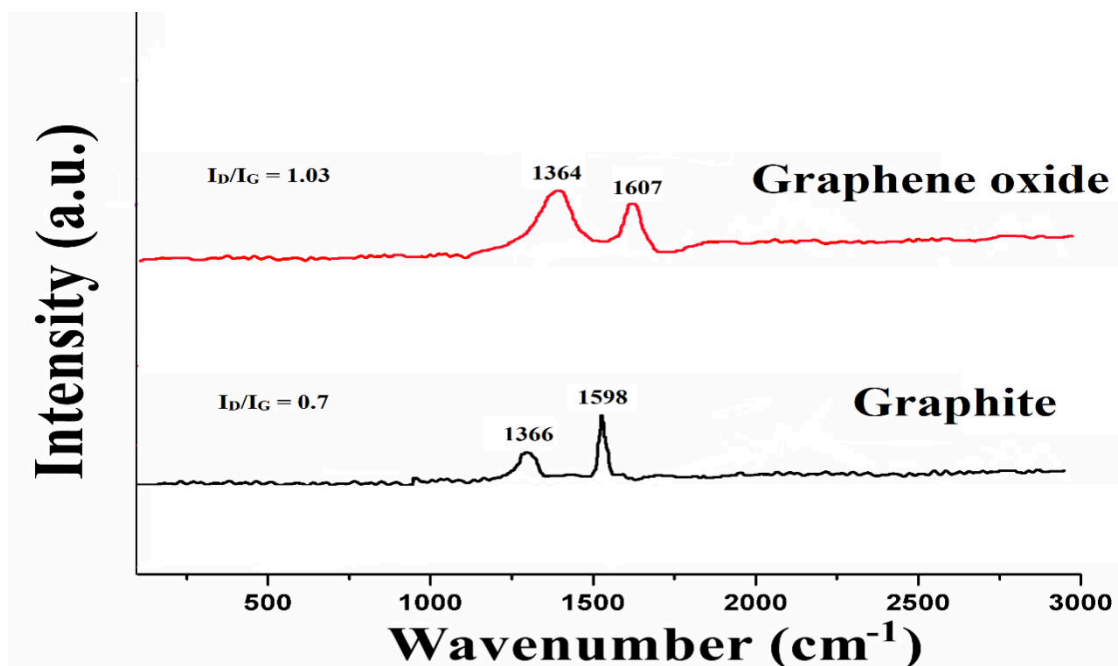


Fig. S2. Raman analysis of Graphite and graphene oxide.

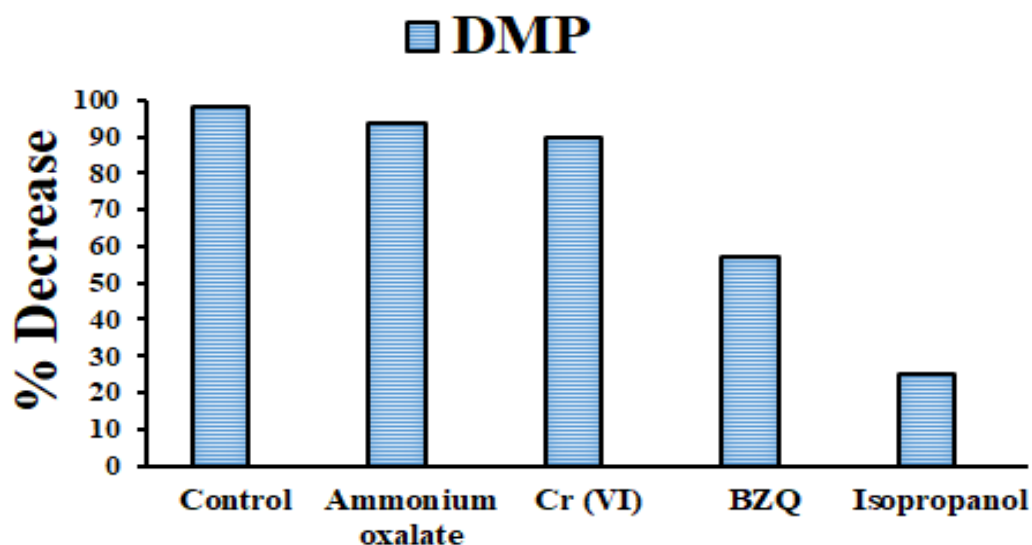


Fig. S3. Effect of radical scavengers on DMP degradation by using  $\text{Eu}^{3+}$ -ZnO/ $\text{Bi}_2\text{O}_3$ /GO.

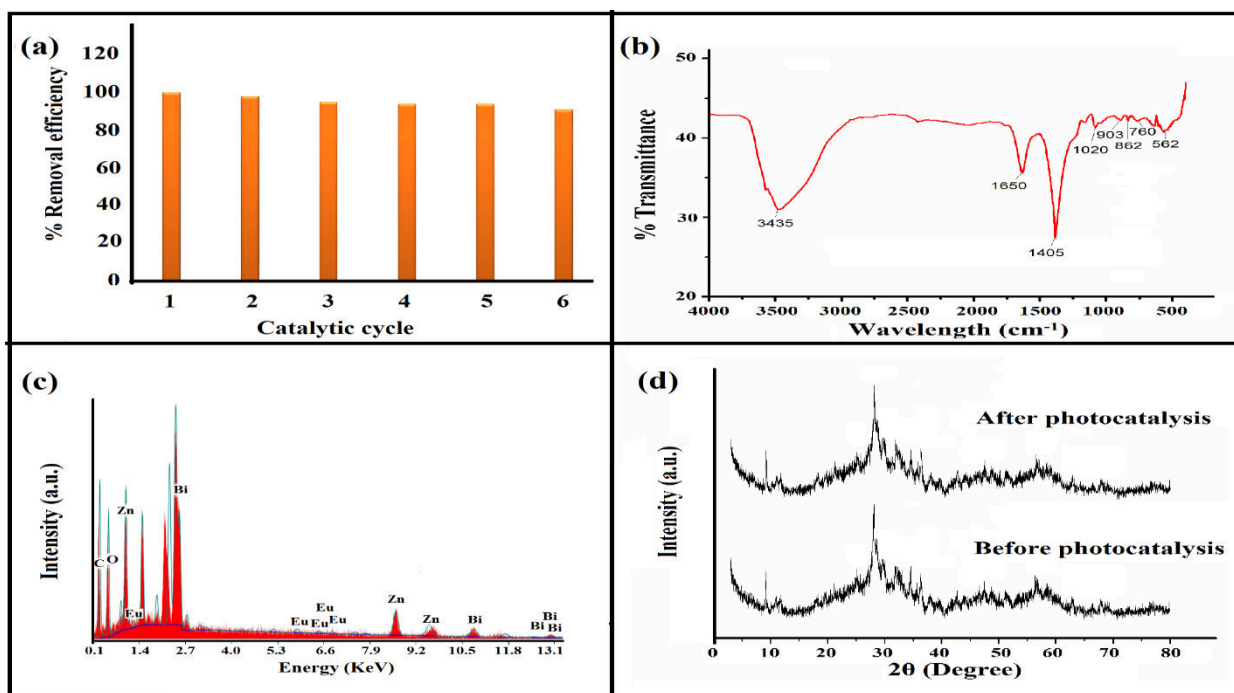


Fig. S4. (a) Recycle efficiency of  $\text{Eu}^{3+}$ -ZnO/ $\text{Bi}_2\text{O}_3$ /GO (b) FTIR spectra of  $\text{Eu}^{3+}$ -ZnO/ $\text{Bi}_2\text{O}_3$ /GO after photocatalysis (c) EDX analysis of  $\text{Eu}^{3+}$ -ZnO/ $\text{Bi}_2\text{O}_3$ /GO after photocatalysis and (d) XRD pattern of  $\text{Eu}^{3+}$ -ZnO/ $\text{Bi}_2\text{O}_3$ /GO before and after photocatalysis [Reaction conditions: initial reaction pH= 4.0; [DMP] =  $1 \times 10^{-3}$  mol  $\text{dm}^{-3}$ ; [photocatalyst] = 50 mg/100 mL; and intensity of light = 750 lx].



2020-03-02

# Synthesis of $\text{Eu}^{3+}$ doped $\text{ZnO}$ heterojunction photocatalyst on graphene oxide sheets for visible light-assisted degradation of 2,4-dimethyl phenol and bacteria killing

Shandilya, Pooja

Elsevier

---

Shandilya P, Sudhaik A, Raizada P, et al., (2020) Synthesis of  $\text{Eu}^{3+}$  doped heterojunction photocatalyst on graphene oxide sheets for visible light-assisted degradation of 2,4-dimethyl phenol and bacteria killing. Solid State Sciences, Volume 102, April 2020, Article number 106164

<https://doi.org/10.1016/j.solidstatesciences.2020.106164>

*Downloaded from Cranfield Library Services E-Repository*